Fractionated Crystallization and Fractionated Melting of Confined PEO Microdomains in PB-*b*-PEO and PE-*b*-PEO Diblock Copolymers

R. V. Castillo,[†] M. L. Arnal,[†] A. J. Müller,*[,†] I. W. Hamley,[‡] V. Castelletto,[‡] H. Schmalz,[§] and V. Abetz[||]

Grupo de Polímeros USB, Departamento de Ciencia de los Materiales, Universidad Simón Bolívar, Apartado 89000, Caracas 1080-A, Venezuela, School of Chemistry, University of Reading, Whiteknights, Reading RG6 6AD, U.K., Makromolekulare Chemie II, Universität Bayreuth, 95440 Bayreuth, Germany, and Institut für Polymerforschung, GKSS-Forschungszentrum Geesthacht GmbH, 21502 Geesthacht, Germany

Received August 21, 2007; Revised Manuscript Received November 19, 2007

ABSTRACT: The confined crystallization of poly(ethylene oxide) (PEO) in predominantly spherical microdomains formed by several diblock copolymers was studied and compared. Two polybutadiene-*b*-poly(ethylene oxide) diblock copolymers were prepared by sequential anionic polymerization (with approximately 90 and 80 wt % polybutadiene (PB)). These were compared to equivalent samples after catalytic hydrogenation that produced double crystalline polyethylene-*b*-poly(ethylene oxide) diblock copolymers. Both systems are segregated into microdomains as indicated by small-angle X-ray scattering (SAXS) experiments performed in the melt and at lower temperatures. However, the PB-*b*-PEO systems exhibited a higher degree of order in the melt. A predominantly spherical morphology of PEO in a PB or a PE matrix was observed by both SAXS and transmission electron microscopy, although a possibly mixed morphology (spheres and cylinders) was formed when the PEO composition was close to the cylinder−sphere domain transitional composition as indicated by SAXS. Differential scanning calorimetry experiments showed that a fractionated crystallization process for the PEO occurred in all samples, indicating that the PE cannot nucleate PEO in these diblock copolymers. A novel result was the observation of a subsequent fractionated melting that reflected the crystallization process. Sequential isothermal crystallization experiments allowed us to thermally separate at least three different crystallization and melting peaks for the PEO microdomains. The lowest melting point fraction was the most important in terms of quantity and corresponded to the crystallization of isolated PEO spheres (or cylinders) that were either superficially or homogeneously nucleated. This was confirmed by Avrami index values of approximately 1. The isothermal crystallization results indicate that the PE matrix restricts the crystallization of the covalently bonded PEO to a higher degree compared to PB.

Introduction

Self-assembly in the melt of block copolymers is induced by microphase separation, creating ordered structures with periodicities on the micro- or nanometer scale that can be used as patterning for different nanotechnology applications. The microdomain (MD) structures are influenced by the composition and the segregation strength between the blocks. In addition, if one or more blocks crystallize, a competition between the driving force of crystallization and phase segregation will then define the final morphology.[1−5] The final morphology of the block copolymer can be determined by the segregation strength (given by χN, the product of the Flory−Huggins interaction parameter χ and the degree of polymerization N), the composition, and the relative magnitudes of three transition temperatures: the order−disorder transition temperature (T_{ODT}), the glass transition temperature (T_g) of the amorphous block, and the crystallization temperature (T_c) of the crystallizable one. Typical cases reported in the literature are (a) *Homogeneous melt* ($T_{ODT} < T_c > T_g$). The microphase separation in this case is driven by the crystallization process if the T_g of the amorphous block is lower than the T_c of the crystallizable block. The resulting MD morphology is usually lamellar and therefore the crystalline lamellae are sandwiched by the amorphous block layers. (b) *Soft confinement* ($T_{ODT} > T_c > T_g$). The segregation strength, χN, will determine the final MD morphology. For weakly segregated systems (with low χN values), the crystallization process will dominate and a "break out" of the melt morphology can occur producing an interconnected morphology that depends on composition. If the copolymers are in the intermediate segregation limit (with intermediate χN values), the MD morphology will depend on the thermal treatment employed during the crystallization process. Finally, for strongly segregated diblock copolymers (with high χN values), the MD morphology will be confined and no break-out can occur. (c) *Hard confinement* ($T_{ODT} > T_g > T_c$). This is a very similar case to the one described in (b) except that since the crystallization occurs at temperatures below T_g of the neighboring block the tendency to keep the melt MD structure is more pronounced and a confined crystallization in MD is usually obtained.[2,6−8]

When a crystallizable polymer is confined to isolated phases (i.e., droplets in immiscible blends) or to the MD morphology of block copolymers (cylinders or spheres), a process named "fractionated crystallization" can arise.[9−10] This means that the crystallization of the polymer MD when it is cooled from the melt does not occur in a single step, as it is usually the case, but rather occurs in several steps or fractions. This is best understood by considering a DSC cooling trace from the melt for a given polymer. Usually any given polymer crystallizes in

* To whom correspondence should be addressed. E-mail: amuller@usb.ve. Fax: 58-212-9063388.
[†] Universidad Simón Bolívar.
[‡] University of Reading.
[§] Universität Bayreuth.
[||] GKSS-Forschungszentrum Geesthacht GmbH.

10.1021/ma0718907 CCC: $40.75
Published on Web 01/03/2008

a single exotherm that occurs at a relatively small supercooling. A polymer may contain several types of heterogeneities depending on its active heterogeneous nuclei densities, let us say A and B, but only the most active ones will be effective in a bulk polymer, i.e., type A heterogeneities. If this polymer is subdivided into many MDs (dispersed in an immiscible matrix), and if the number of MDs is larger or of the same order of magnitude as the number of heterogeneous nuclei available in the bulk polymer, a certain population of the MDs will remain without heterogeneities. Other fractions may contain type A heterogeneities, while yet another may contain type B heterogeneities. As a result, when such a dispersion is cooled from the melt, the MD population that contains type A heterogeneities will crystallize at the same crystallization temperature as the bulk polymer (usually at small supercoolings) in a first exotherm whose size is proportional to the number of MD that can crystallize at such temperatures. The MD population that contains the less active type B heterogeneities can only crystallize at larger supercoolings in a second exotherm. Finally, the MD population that is free of heterogeneities will crystallize at the maximum possible supercooling in a third exotherm originated from either superficially generated nuclei (at the interface) or homogeneous nuclei.[2] In this way, such a hypothetical dispersion of MDs would display three distinct exotherms upon cooling from the melt instead of one for an equivalent bulk polymer.

Block copolymers could be considered as ideal systems to study homogeneous nucleation because of their purity and the ability to form a very large number of MDs of very small dimension. However, the covalently bonded chains, variable segregation strength (which depends on χN), and composition define the morphology of the MD and also the possibility that these may be percolated. If the MDs are percolated, secondary nucleation will spread throughout and the fractionated crystallization phenomena could be reduced or even totally absent. The probability of percolation decreases in the order lamellae > cylinder > spheres.[2] In the case of isolated spherical microdomains, the crystallization kinetics is usually dominated by nucleation and first-order kinetics have been observed corresponding to values of the Avrami index of 1.[2,11] Values <1 in Avrami indexes have been interpreted as indications of having not fully sporadic nucleation processes but closer to instantaneous.[12] Finding Avrami indexes of 1 or less cannot be regarded as a proof of homogeneous nucleation since superficial nucleation cannot be ruled out easily. If Avrami indexes of 1 or lower are encountered and the crystallization is occurring at the maximum possible supercooling, i.e., at a few degrees above T_g, then homogeneous nucleation is probably occurring. Fractionated crystallization as well as homogeneous nucleation in block copolymers have been recently reported and reviewed.[2,7,13−19]

Recent reviews and reports on the properties of crystalline−amorphous and crystalline−crystalline diblock copolymers have been published.[2,20−23] Chen et al.[24] found a dramatic reduction in crystallization temperature of poly(ethylene oxide), PEO, with the change in MD morphology from bulk through spheres (bulk, lamellae, cylinders, and spheres) in blends of polybutadiene (PB) and PB-*b*-PEO diblock copolymers. A dependence of the homogeneous nucleation temperature on the volume of the crystallizing phase is also expected for isolated MDs.[25] The spheres can deform into ellipsoid-like objects due to PEO crystallization.[26] However, large scale deformation was not detected by Reiter et al.[27] These authors[27] and Röttele et al.[28] reported that PEO crystals nanoconfined in a PB matrix are highly imperfect and display significant reorganization phenomena during heating. PEO spheres within PB matrices in block copolymers have also been studied by Huang et al.,[29,30] and the systems with 17 wt % PEO were considered to be close to the cylindrical−spherical domain transition. As a consequence, slight perturbations in interfacial curvature may be enough to produce domain coalescence to reduce the interfacial energy.

To our knowledge, PE-*b*-PEO systems have not been extensively studied. Sun et al.[31] studied low molecular weight PE-*b*-PEO block copolymers. Extended-chain crystals were obtained for both blocks in a lamellar morphology. Additionally, a reduction of the crystallization rate of the PEO block was obtained as a consequence of nanoconfinement of PEO blocks between PE crystalline lamellae. A "pathway-dependent melting process" was reported for the same system.[32] Boschetti-de-Fierro et al.[33] have studied poly(1,4-butadiene)-*b*-polystyrene-*b*-poly(ethylene oxide) (PB-*b*-PS-*b*-PEO) triblock terpolymers and their hydrogenated counterparts PE-*b*-PS-*b*-PEO by small-angle X-ray scattering (SAXS), transmission electron microscopy (TEM), and differential scanning calorimetry (DSC). The crystallization and melting of the PEO and PE blocks were dependent on the volumetric composition and molecular weight.

Schmalz et al.[7,19] synthesized poly(1,4-butadiene)-*b*-poly(1,4-isoprene)-*b*-poly(ethylene oxide) (PB-*b*-PI-*b*-PEO) and its hydrogenated version PE-*b*-PEP-*b*-PEO. The crystallization and selfnucleation of the crystallizable blocks were a function of the triblock terpolymer morphology. When the crystallizable phases were confined, the selfnucleation regime (regime II) disappeared and the crystallization occurred at very large supercoolings.

In this work, the crystallization of predominantly PEO spheres formed by several diblock copolymers was studied and compared. Two polybutadiene-*b*-poly(ethylene oxide) diblock copolymers were prepared by sequential anionic polymerization techniques (i.e., B_{89}-*b*-EO_{11}^{102} and B_{81}-*b*-EO_{19}^{34}, wherein the subscript indicates the composition by weight and the superscript the number average molecular weight of the block copolymer in kg/mol). These were compared to equivalent samples after catalytic hydrogenation that produced double crystalline polyethylene-*b*-poly(ethylene oxide) diblock copolymers (i.e., E_{89}-*b*-EO_{11}^{102} and E_{82}-*b*-EO_{18}^{34}). These samples were also subjected to annealing treatments to evaluate possible changes in their morphology. As a result, the crystallization of PEO spheres in a rubbery (PB) or a semicrystalline matrix (PE) could be studied and compared.

Experimental Part

Synthesis. Solvents and monomers for anionic polymerization were purified according to common procedures described elsewhere.[7,34,35] Briefly, the synthesis of poly(1,4-butadiene)-*b*-poly(ethylene oxide) (PB-*b*-PEO) diblock copolymers and Poly(1,4-butadiene) (PB) homopolymer was accomplished by sequential anionic polymerization of butadiene and ethylene oxide in benzene at 60 °C using *sec*-BuLi as the initiator. Polymerization of ethylene oxide in the presence of a lithium counterion was realized by using the recently established strong phosphazene base *t*-BuP_4 (Li^+:*t*-BuP_4 = 1:1). The polymerization of ethylene oxide was complete after 3 days and was terminated with a mixture of methanol/acetic acid (1/5, v/v) followed by precipitation in methanol.[7]

Hydrogenation. The polyethylene-*b*-poly(ethylene oxide) (PE-*b*-PEO) diblock copolymers and PE (PE) homopolymer were obtained by hydrogenation of the corresponding precursors PB-*b*-PEO and PB. Homogeneous catalytic hydrogenation was carried out in degassed toluene (1.5−2 wt % solution of the polymer) at 60 °C and 60 bar H_2 pressure for 3−4 days using Wilkinson catalyst $(Ph_3P)_3Rh^{I}Cl$ (1 mol % with respect to the number of double bonds

Table 1. Molecular Characteristics of the Block Copolymers and Homopolymers Employed in This Work

	PB block		PEO block	
sample	$\overline{M_n}$ (g/mol)	% 1,2 units	$\overline{M_n}$ (g/mol)	d.i.
PE^{25}	25 000	11		1.01
PEO^{1}			1000	
$B_{81}EO_{19}{}^{34}$	27 800	13	6700	1.02
$E_{82}EO_{18}{}^{35}$	28 700		6300	
$B_{89}EO_{11}{}^{102}$	90 200	12	11 500	1.02
$E_{89}EO_{11}{}^{105}$	93 450		11 550	

of the PB block). Under the employed conditions, the PB block gets completely hydrogenated as revealed by ^{1}H NMR (Bruker AC 250 spectrometer). Purification was accomplished by precipitation into isopropanol. Further purification was performed in order to remove the residual Wilkinson catalyst by refluxing a homopolymer or block copolymer solution in toluene with a small amount of concentrated hydrochloric acid followed by precipitation into isopropanol.[7]

The molecular characteristics of the block copolymers and homopolymers are reported in Table 1. A neat PE (M_n = 25 000 g/mol) and a PEO standard (M_n = 1000 g/mol) were employed for qualitative comparison. The neat PE is a hydrogenated polybutadiene with a high content of 1,4-addition (11 mol % of 1,2 units). It can be considered as a random copolymer of ethylene and 1-butene, where the ethyl branches are not incorporated in the PE crystals thereby limiting the maximum possible lamellar thickness. The 1,2-units content for the PE blocks within the PE-*b*-PEO diblock copolymers is also reported in Table 1, as it will have an influence on the crystallization and especially on the melting temperature of the PE crystals.

Small-Angle and Wide-Angle X-ray Scattering. Simultaneous small-angle and wide-angle X-ray scattering experiments were carried out at the Synchrotron Radiation Source, Daresbury Lab, U.K. on station 6.2.[36,37] DSC pans modified to incorporate mica windows to allow transmission of the X-ray beam were employed to contain the samples and were mounted in a Linkam DSC cell of single pan design for thermal treatment. The X-ray wavelength was λ = 1.40 Å. SAXS wavenumber ($q = 4\pi\sin\theta/\lambda$) was calibrated using rat-tail collagen, and the WAXS angular scale was calibrated using the reflections of high-density polyethylene (HDPE). SAXS data were registered with a RAPID multiwire quadrant detector, and the WAXS detector had a curved multiwire design.

Differential Scanning Calorimetry. A Perkin-Elmer Pyris 1 instrument was employed. Samples of approximately 10 mg were encapsulated in aluminum pans. The calibration was performed with indium and tin, and all tests were run employing ultrapure nitrogen as purge gas. Standard DSC heating and cooling scans were performed at 10 °C/min. Isothermal step crystallizations (ISC) experiments were employed and the detailed procedure is explained as follows.[38] The sample was melted at 120 °C for 3 min. Then, it was quenched from the melt (at 60 °C/min) to the first crystallization temperature, T_c, and it was held at this first T_c for a given crystallization time, t_1. Then the sample was heated from T_{c1} to 120 °C at 10 °C/min. The heat of fusion was determined, and it was supposed to be equal to the heat of crystallization developed during the isothermal crystallization step applied at t_1. The procedure was repeated successively varying the isothermal crystallization time until enough data were collected to determine the isothermal crystallization kinetics at T_{c1}. Then a different crystallization temperature was chosen and the whole process was repeated at different times.

Transmission Electron Microscopy. The bulk morphology of the PE-*b*-PEO and PB-*b*-PEO diblock copolymers was examined in a JEOL 1220 TEM operated at 100 kV. Small pieces of the diblock copolymers were first stained by immersing in 1% RuO_4 stabilized aqueous solution or by exposing to OsO_4 vapor (for the polybutadiene systems). After the staining process, small pieces were sectioned in a LEICA M3Z ultramicrotome at −90 °C. Ultrathin sections of approximately 50 μm were obtained using a diamond knife and were stained again by vapors of the staining agent.

Micrographs were obtained from which the average number and volume diameters (d_n and d_v) of the particle cross-sections were determined by measuring and counting at least 100 particles. The dispersity (D) of the sizes obtained and the average number of particles/cm^3 were also calculated. The number and volume average diameters were obtained using the following equations:[39]

$$d_n = \frac{\sum n_i d_i}{\sum n_i} \quad (1)$$

$$d_v = \frac{\sum n_i d_i^4}{\sum n_i d_i^3} \quad (2)$$

where n_i is the number of droplets, i, of diameter d_i.

The particle size polydispersity was evaluated by means of:

$$D = d_v/d_n \quad (3)$$

The volume fraction of the dispersed phase was calculated from the following relationship:

$$X_v = (X_d/\rho_d)/[X_d/\rho_d + (1 - X_d)/\rho_m] \quad (4)$$

where X_d is the weight fraction of the dispersed phase, ρ_d is the dispersed phase density, and ρ_m is the matrix density.

The average particle number per cm^3 was determined from:

$$N_i = X_v/(\pi/6(d_n)^3) \quad (5)$$

The samples were also subject to an annealing thermal treatment in an inert atmosphere at 140 °C for 4 h. These samples are denoted as $a\mathrm{A}_x\mathrm{B}_y{}^m$.

Results and Discussion

Morphological Characterization. The bulk morphology of the PE-*b*-PEO and PB-*b*-PEO diblock copolymers was studied by TEM, and the micrographs are presented in Figure 1. A predominantly spherical morphology was revealed with PEO spheres in a PB or a PE matrix. The spherical morphology for the PB-*b*-PEO diblock copolymers was revealed by OsO_4 staining and although the general morphology is that of disordered isolated spheres, some groups of percolated spheres (or spheres forming trains) can be visualized (Figures 1a, 1b).

In the case of the $B_{81}EO_{19}{}^{34}$ and $E_{82}EO_{18}{}^{35}$ copolymers, the composition is close to the sphere-cylinder transitional composition and some of the groups of percolated spheres may be the precursors of the cylinders. SAXS studies below will show that a mixture of spheres and cylinders may be present for these diblock copolymers. The sphere diameters were measured from the micrographs and are reported in Table 2. The mean number and volume diameter exhibit differences that could indicate that the morphology is not perfectly regular. This could correspond to a nonequilibrium morphology or a transitional morphology in between spheres and cylinders, in particular for $B_{81}EO_{19}{}^{34}$ and $E_{82}EO_{18}{}^{35}$.

Huang et al. reported a somewhat similar behavior[30] for a PB-*b*-PEO block copolymer with 17 wt % PEO and molecular weight of 6800 g/mol. They found PEO spherical domains with poor long-range order as revealed by TEM and SAXS. SAXS profiles for amorphous and isothermically crystallized samples showed a broad primary peak attributed by the authors to spherical microdomains without a defined pattern. The lack of long-range order was attributed to the fast solvent casting

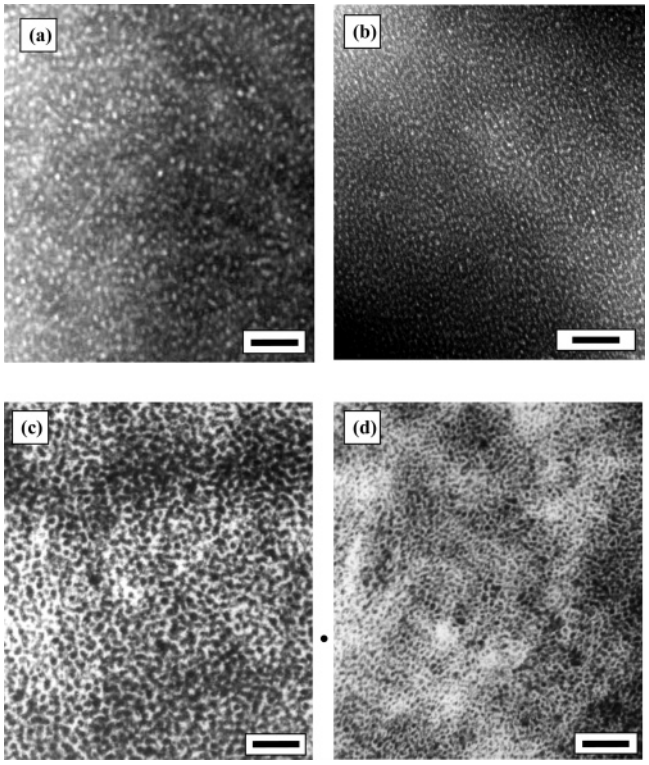

Figure 1. TEM micrographs of PB-*b*-PEO and PE-*b*-PEO diblock copolymers: (a) $B_{89}EO_{11}^{105}$; (b) $B_{81}EO_{19}^{34}$; (c) $E_{89}EO_{11}^{105}$; (d) $E_{82}EO_{19}^{35}$. Scale bar = 200 nm.

Table 2. Sphere Dimensions Obtained by TEM Measurements and SAXS Calculations

	TEM		SAXS	
sample	$d_n/d_v/D$ (nm/nm/±)	$X_v/N_i{}^a \times 10^{-16}$ (cm^{-3})	d (nm)	$X_v/N_i \times 10^{-16}$ (cm^{-3})
$B_{81}EO_{19}^{34}$	13/17/1.3	0.16/6.16		
$B_{89}EO_{11}^{102}$	19/27/1.4	0.09/0.9	20.4	0.09/2.02
$E_{82}EO_{18}^{35}$	21/22/1.0	0.15/2.6		
$E_{89}EO_{11}^{105}$	31/32/1	0.09/0.5	29	0.09/0.70

[a] N_i = number of microdomains per cm^3.

process and to the slow dynamics of the rearrangement of microdomains into the equilibrium lattice because of relatively long PB block length. SAXS results also indicated perturbation of the melt morphology after crystallization by coalescence of the spheres.

It can be appreciated that as expected the sphere diameters obtained by TEM for the copolymer with the longer PEO chains ($B_{89}EO_{11}^{102}$) are larger (see Table 2) than those obtained for the lower molecular weight sample ($B_{81}EO_{19}^{34}$). The PEO sphere dimensions are in the same order of magnitude as those reported for similar block copolymers of similar systems taking into consideration their molecular weight.[24,28−30]

Panels c and d of Figure 1 show micrographs corresponding to the PE-*b*-PEO diblock copolymers. In this case, RuO_4 was employed as a staining agent with very long exposure times, ca. 1 week. We believe that the PEO spheres and the amorphous regions close to their interphase were stained since the PEO spheres appear larger (see Table 2) than those in the corresponding PB-*b*-PEO copolymers of equivalent compositions (i.e., the same materials without hydrogenation). Once more, disordered patterns were present for both systems and could not be improved by annealing treatments; TEM revealed no major changes in the bulk morphology for the annealed samples (results not shown). The hydrogenated systems clearly presented

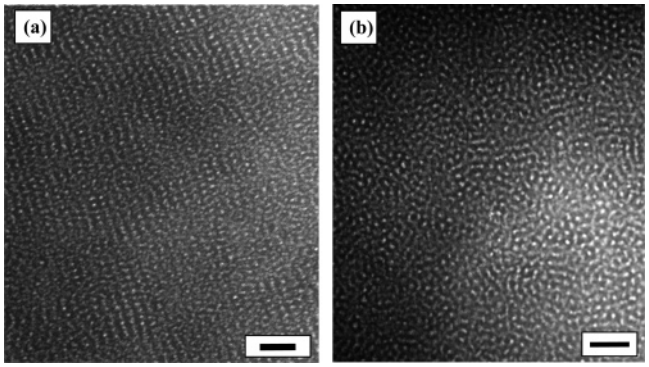

Figure 2. TEM micrographs of annealed PB-*b*-PEO diblock copolymers: (a) $B_{89}EO_{11}^{105}$; (b) $B_{81}EO_{19}^{34}$. Scale bar = 200 nm.

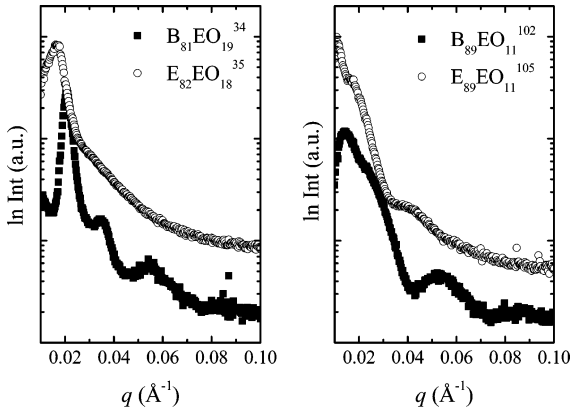

Figure 3. SAXS patterns at 120 °C for the indicated PB-*b*-PEO and PE-*b*-PEO diblock copolymers.

a slower dynamics, disturbing chain diffusion, and rearrangement of MDs compared to the PB-*b*-PEO copolymers.

In the case of PB-*b*-PEO samples, the morphology was slightly improved by annealing at 140 °C for 4 h. For *a*$B_{89}EO_{11}^{102}$ and *a*$B_{81}EO_{19}^{34}$, TEM revealed a higher long-range order microdomain geometry (see Figure 2) compared to unannealed samples (Figure 1). A peculiar long-range order of spherical microdomains can be seen for the *a*$B_{89}EO_{11}^{102}$ diblock copolymer sample in Figure 2a, in which the spheres are arranged in trains despite some apparent disordered regions, which could be artefacts induced by ultramicrotomy. A TEM micrograph for *a*$B_{81}EO_{19}^{34}$ diblock copolymer sample is shown in Figure 2b, in which a pseudo "hexagonally packed spheres" pattern is observed in some areas, but some percolated microdomains apparently coexist with this morphology. This hexagonal-like pattern may indicate the coexistence with cylinders, although a lateral view of these cylinders was not observed by TEM. This coexistence phenomenon could be a consequence of the critical composition (19 wt % PEO) present in $B_{81}EO_{19}^{34}$ which is close to the spheres−cylinders domain transitional composition. Dimensions of the microdomains remain unaltered with respect to the nonannealed PB-*b*-PEO diblock copolymers.

The predominant PEO spherical morphology in a PB or a PE matrix for the studied copolymers was studied by SAXS. SAXS profiles were taken at 120 °C for the two types of diblock copolymers (PB-*b*-PEO and PE-*b*-PEO) and they are presented in Figure 3. The first maxima of the samples correspond to the primary lattice peak; the other scattering maxima are the form factor peaks related to scattering from isolated microdomains.[30] The form factor scattering depends on the microdomain geometry, including the shape, the average dimension, and the dimension distribution.[40]

Table 3. Values of χN Calculated Using Different Solubility Parameters at Different Temperatures for the PB-*b*-PEO and PE-*b*-PEO Diblock Copolymers

		solubility parameters $(cal/cm^3)^{1/2}$ (PB−PEO)				solubility parameters $(cal/cm^3)^{1/2}$ (PE−PEO)		
		8.6−9.73	7.16−8.7	8.6−10.4		8.21−9.73	7.7−8.7	8.0−10.4
sample	T(°C)	χN	χN	χN	sample	χN	χN	χN
	25	79	149	216		171	74	428
$B_{81}EO_{19}^{34}$	80	67	125	183	$E_{82}EO_{18}^{35}$	145	63	361
	120	60	113	164		130	56	324
	25	241	452	657		468	203	1170
$B_{89}EO_{11}^{102}$	80	203	381	555	$E_{89}EO_{11}^{105}$	395	171	987
	120	183	342	498		355	154	887

The SAXS trace for the $B_{89}EO_{11}^{102}$ copolymer could be successfully fitted to a microphase-separated spherical structure (PEO spheres), and the dimensions of the spheres are reported in Table 2 and are in agreement with the dimensions obtained by TEM. However, the $B_{81}EO_{19}^{34}$ SAXS profile does not fit very well to a spherical morphology, and the data indicate a mixture of cylinders and spheres. The SAXS experiments were repeated with the annealed samples but the resolution of the patterns obtained did not improve significantly. If the SAXS data for $B_{81}EO_{19}^{34}$ is fitted to a sphere model, the mean value for the diameter of the spheres obtained is almost twice than that obtained by TEM. Therefore, no values are reported in Table 2 for this copolymer and its hydrogenated counterpart. As stated previously, this system has a composition with 19 wt % of PEO, which is close to the composition at which sphere−cylinder transition takes place. This complex behavior makes SAXS interpretation difficult possibly because of the coexistence of spherical and cylindrical microdomains and a higher fraction of percolated spheres (evidenced by TEM); these yield average dimensions that can cause poor fitting of the experimental data. In TEM, only isolated "spheres" were considered for calculation of the values shown in Table 2.

In the case of the PE-*b*-PEO diblock copolymers, the SAXS patterns are less resolved (see Figure 3). The intensity of the form factor shoulder at $q = 0.035$ Å^{-1} changes on crystallization. However, it is clear that a lamellar superstructure is not formed because the peak positions do not change into equally spaced peaks of a lamellar structure. The change in intensity of the shoulder peak may reflect changes in the electron density on crystallization or slight distortion of the spherical domains.

Both types of block copolymers can be regarded as strongly segregated as judged by their values of $\chi N > 50$ (see Table 3). However, the values of χN for similar composition PB-*b*-PEO and PE-*b*-PEO copolymers depend on the values of the solubility parameters (i.e., δ) chosen to calculate χ. Table 3 reports several values of segregation strength that correspond to calculations performed employing the highest and the lowest δ values reported in the literature (columns 1 and 2) and the values calculated by Van Krevelen's group contribution theory (column 3 and ref 41). Comparison of all the values obtained reveals that it is not possible to reach a conclusion about which of the systems is more segregated in the melt than the other, since the solubility parameters cannot be conclusively determined and they fall in a very similar range of values. Furthermore, Almdal et al.[42] evaluated the segment−segment interaction parameters of several symmetric diblock copolymers and how they are affected by variations in local chain structure. They suggest that for PEO−hydrocarbon block copolymers an enthalpic contribution to the χ parameter is present that depends on the conformational asymmetry which is not considered by Flory−Huggins theory. Accordingly, the interaction parameters cannot be predicted by using a common set of solubility parameters. Experimental measurements of the order−disorder transition temperatures (ODT) for these systems were not possible to perform because the degradation of the PEO block started before the ODT temperature was reached.

Nevertheless, the SAXS evidence presented in Figure 3 suggests that the PB-*b*-PEO diblock copolymers are better ordered in the melt than the PE-*b*-PEO samples. This is quantified by the pronounced structure factor peaks for the PB-*b*-PEO samples. Additionally, TEM results for the annealed samples showed improvement in the long-range order in PB-*b*-PEO but not in PE-*b*-PEO diblock copolymers. SAXS patterns during cooling from the melt were recorded at different temperatures and are shown in Figures 4 and 5 for two selected samples. Figure 4 contains the SAXS data taken at 120, 50, 5, and −18 °C for $B_{81}EO_{19}^{34}$. The patterns clearly show that the morphology is not substantially altered after the crystallization of the PEO microdomains under PB soft confinement. The subtle changes in the SAXS reflections may be connected to the small deformation of the MD but no clear trend was observed as a function of temperature. Figure 5 shows similar data for $E_{89}EO_{11}^{105}$. In this case, the form factor peaks are more affected by PEO and PE crystallization and clear broadening of the maximum around $q = 0.05$ Å^{-1} can be observed. Nevertheless, the melt morphology is still retained after the crystallization of both the PEO spheres and the PE matrix. The crystallization of the PEO spheres is also occurring under relatively soft confinement, since the amount of crystallinity developed by the PE

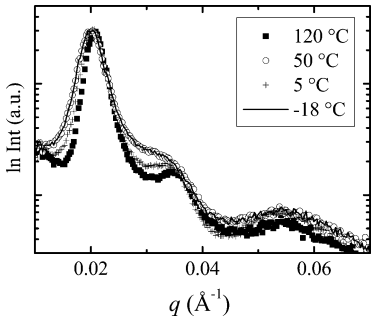

Figure 4. SAXS patterns at different temperatures for the $B_{81}EO_{19}^{34}$ diblock copolymer.

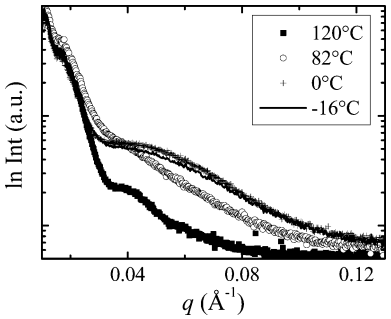

Figure 5. SAXS patterns at different temperatures for the $E_{89}EO_{11}^{105}$ diblock copolymer.

Table 4. Thermal Properties for the Diblock Copolymers and Homopolymers Obtained from Figures 5 and 6

	PE block						PEO block								
			T_c (°C)				ΔH_c (J/g)				T_c (°C)				
sample	α ΔH_c (J/g)	ΔH_m (J/g)	α	β	T_m (°C)	X_c (%)	A	B	C	ΔH_m (J/g)	A	B	C	T_m (°C)	X_c (%)
PE^{25}	60	89	87.1	51.7	98.8	20									
PEO^{1}										143	21.0			40.0	73
PEO^{2}							158			166	29.8			54.7	80
$B_{81}EO_{19}^{34}$							3	4	82	145	46.1	−8.2	−27.1	56.1 61.3	45
$E_{82}EO_{18}^{35}$	53		77.7	75.0	93.6	18	14	4 7	50		45.7	20.2 −1.0	−34.3	45.0	38
$B_{89}EO_{11}^{102}$								1	81	134		−11.5	−26.8	56.7 61.6	42
$E_{89}EO_{11}^{105}$	47		76.2	53.1	91.4	16		3	58			0.5	−24.3	52.6 57.5	31

(the first polymer to crystallize upon cooling from the melt at 82 °C in Figure 5) was estimated by DSC to be between 16 and 18% for $E_{82}EO_{19}^{35}$ and $E_{89}EO_{11}^{105}$ (see Table 4), leaving most of the matrix in the amorphous rubbery state. Even if the DSC values may contain errors due to the overlap of signals, it would be difficult for the crystallinity values to be above 30% and still 70% of the matrix would be composed of rubbery PE chains.

Thermal Characterization. The thermal behavior of the examined diblock copolymers and in particular the crystallization process of the PEO block will be affected by the confinement, the characteristics of the interphase, and the molecular weight of the PEO block under study. In the case of the PE block that forms the matrix in PE-*b*-PEO diblock copolymers, its crystallization and melting processes depend mainly on the short chain branching content (i.e., the 1,2-units content in the high 1,4-PB precursor).

Standard DSC Scans. Figure 6 shows the DSC cooling scans of the copolymers and representative homopolymers. The DSC cooling scans of $B_{81}EO_{19}^{34}$ and $B_{89}EO_{11}^{105}$ display three and two crystallization exotherms, respectively, (their peak values are reported in Table 4). This is a consequence of the confinement of PEO microdomains, of which a small population is percolated. Therefore, fractionated crystallization takes place as described in the introduction.

The number of PEO MDs is very high in sphere-forming diblock copolymers. In the present case, it is in the order of 10^{16} spheres/cm^3 (see actual values in Table 2) while the typical type A heterogeneity content (i.e., highly active heterogeneities that provoke nucleation at low supercoolings) in PEO is in the order of 10^6 heterogeneities/cm^3, as ascertained by polarized light optical microscopy experiments. This means that there will be a vast number of PEO spheres or microdomains without type A heterogeneities, leaving them with type B heterogeneities (less active heterogeneities that can only nucleate at intermediate supercoolings) or without any heterogeneity whatsoever. Heterogeneity-free spheres can only undergo surface nucleation (i.e., nucleation that starts at the interphase between the blocks) or truly homogeneous nucleation (i.e., spontaneous aggregation of PEO chains to form nuclei).[2,18] When the spheres are isolated, crystal growth cannot advance from one MD to the next and each sphere will need its own nucleus. On the other hand, if they are percolated, secondary nucleation can spread through out that region or group of spheres.

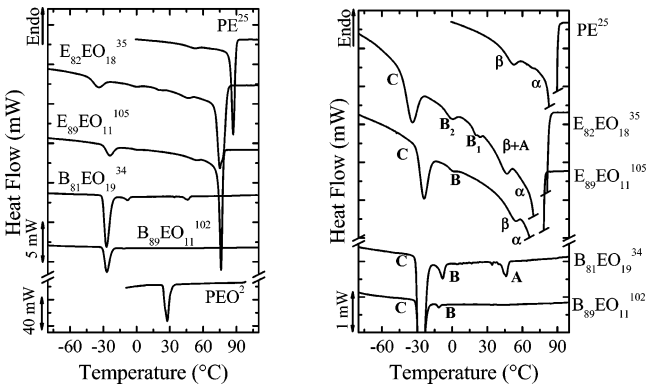

Figure 6. DSC cooling scans at 10 °C/min after melting at 120 °C for the indicated PB-*b*-PEO and PE-*b*-PEO diblock copolymers. Right: close up of the left side figure. See text for details.

In the case of $B_{81}EO_{19}^{34}$, the small exotherm that peaks at 46 °C corresponds to the crystallization after highly efficient nucleation by type A heterogeneities, since it appears at low supercoolings at temperatures similar to those exhibited by a PEO homopolymer of equivalent molecular weight (result not shown here). This exotherm represents only 3% of the entire latent crystallization enthalpy of the PEO block. At intermediate supercoolings, a second minor exotherm (see Figure 6b for a close-up and Table 4 for temperature values) corresponding to just 5% of the total enthalpy of crystallization peaks at −8.2 °C and has been labeled with the letter B to indicate that it probably arises from the nucleation caused by less active heterogeneities. (Percolated spheres or small cylinders, most likely crystallized either in exotherm A or B.) Finally, at −27 °C (peak crystallization temperature reported in Table 4), a sharp exotherm corresponding to 92% of the crystallization enthalpy can be clearly observed, i.e., exotherm C. Such a low-temperature crystallization could indicate homogeneous or superficial nucleation. In this case, it could correspond to the crystallization of heterogeneity-free, isolated PEO microdomains that have been nucleated by the interphase or surface of the MDs. This interpretation is based on previous reports that have encountered crystallization of PEO nanospheres at even lower temperatures (from −30 to −40 °C) despite having similar sizes to those presented here.[2,18] The homogeneous nucleation temperature is believed to be the one located closest to the T_g of the crystallizing phase (when comparing identical droplet sizes). Otherwise, superficial nucleation effects may be playing a role in the nucleation process. The T_g of the PEO phase was not observed by DSC (possibly because of the low PEO content in the copolymers and because of its high crystallinity in the homopolymer). However, the T_g values of PEO have been reported and they range from −50 to −60 °C depending on the molecular weight.[2,18] The fact that in exotherm C only the isolated MDs crystallize will be demonstrated by the isothermal crystallization kinetics, which resulted in a first-order process.

In the $B_{89}EO_{11}^{102}$ system, a similar behavior is observed except that exotherm A is not present. Although they have similar crystallinity contents, 42 and 45%, respectively, according to Table 4, exotherm C appears smaller in size in this case than for $B_{81}EO_{19}^{34}$ in view of the differences in composition and morphology observed by SAXS and TEM. The soft confinement provided by the PB matrix and the strong segregation strength result in a substantial reduction in crystallinity content for the PEO block MD compared to the bulk PEO homopolymer (typical crystallinity of PEO homopolymer ranges from 70 to 80% depending on the molecular weight, see also Table 4).

The PE^{25} sample crystallizes with a bimodal exotherm containing two minima labeled α and *β* in Figure 6b. The sharp α peak corresponds to the main crystallization event at 87 °C associated with the crystallization of the longest methylene sequences within the chains. Since the sample contains short ethyl branches, they produce a random distribution of methylene linear sequences of varying length that normally crystallize according to their lengths, i.e., the shorter the sequence the lower the crystallization temperature on a cooling scan. This is the origin of the extended low-temperature tail that can be observed after the sharp α peak in the DSC trace. The *β* peak is usually present in all ethylene/α-olefin copolymers and is attributed to intramolecular crystallization of short linear methylene sequences.[43,44] The crystallinity of the sample is only 20% because of the 1,2-units content (see Tables 1 and 4). In Table 4, the enthalpy of crystallization of PE homopolymer and PE blocks were calculated taking into consideration only the α peak because of the overlap of the *β* peak and type-A crystallization exotherms for PEO blocks within $E_{82}EO_{18}^{35}$.

In the case of PE-*b*-PEO diblock copolymers, both blocks are able to crystallize upon cooling from the melt. The main crystallization temperature for the PE block in both copolymers (α peak) is substantially reduced compared to PE.[25] This is mainly due to the higher 1,2-units content in the PB precursors (see Tables 1 and 4).

For the PE-*b*-PEO copolymers, the fractionated crystallization of the PEO still holds but the number of exotherms and their peak crystallization temperatures change compared to PB-*b*-PEO. Upon hydrogenation, Wilkinson catalyst residues can remain in the system despite attempts to remove them (for more details see ref 18). This could be the reason why the B exotherm splits into B1 and B2 in the $E_{82}EO_{18}^{35}$ case. Also, somewhat lower crystallinity PEO spheres were obtained when the matrix was composed of PE instead of PB (see Table 4). However, the main crystallization event for the PEO MD, even after the PE block has crystallized (see Table 4), within the PE-*b*-PEO diblock copolymer samples is still the C exotherm (95 and 67% of the total PEO crystallization enthalpy occurs within the C exotherm for $E_{89}EO_{11}^{105}$ and $E_{82}EO_{18}^{35}$, respectively). This means that the majority of the PEO MD is isolated and is nucleating either homogeneously or at the surface. This result implies that the PE matrix cannot nucleate the majority of the PEO spheres (and/or cylinders). In fact, the interphase is probably constituted of amorphous rubbery PE chains in view of the low crystallinity value of the PE matrix.

Figure 7 shows the DSC subsequent heating scans that were applied to the samples after the controlled cooling scans shown in Figure 6. The melting behavior of the PE^{25} and the PE block within the PE-*b*-PEO samples reflects their respective crystallization behavior (they are broad and exhibit a wide low-temperature tail due to their 1,4-unit contents) and is dominated by the ethylene branches that interrupt the linear methylene

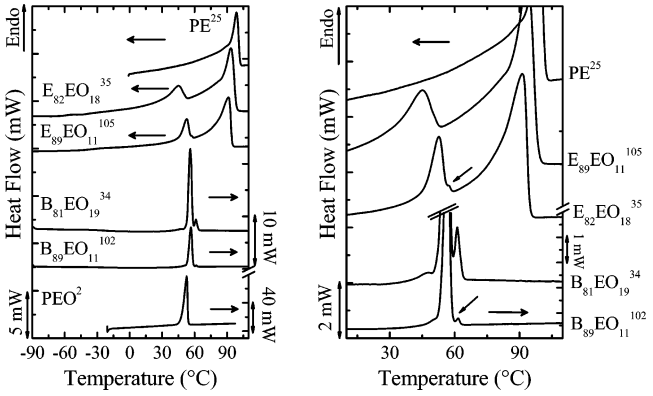

Figure 7. DSC heating scans at 10 °C/min after melting at 120 °C for the indicated PB-*b*-PEO and PE-*b*-PEO diblock copolymers. Right: close up of the left side figure. See text for details.

sequence length. The PEO homopolymer behaves as expected with a rather sharp melting endotherm characteristic of a sample with a narrow molecular weight distribution (see Table 1).

The most interesting and novel behavior was observed for the PEO blocks within $B_{81}EO_{19}^{34}$, $B_{89}EO_{11}^{102}$, and $E_{89}EO_{11}^{105}$, for which double melting peaks were observed. In the case of $E_{82}EO_{18}^{35}$, this effect was not observed since it is probably masked by the overlap of the PE block melting. It should be noted that the most intense endotherm for each run appears at lower temperatures compared to that of the very small second melting process. The first endotherm corresponds to the melting of the crystals within the majority of the MD that crystallize at the lowest temperature in C exotherms as shown in Figure 6. The second and very small melting point corresponds to the melting of the PEO MD that can crystallize at lower supercoolings in exotherms A and B. The metastability of the PEO crystals formed within the nanospheres is clearly indicated by the large differences between crystallization and melting temperatures.

This fractionated melting behavior will be further explored below by sequential isothermal crystallization of different populations of PEO spheres. It is interesting to note that in previous works where fractionated crystallization has been observed, in both blends and block copolymers, reorganization during the subsequent heating scans usually produced a single melting endotherm (see refs 9,15, and 18). So, while fractionated crystallization has been widely observed in the literature, this is the first time that a subsequent fractionated melting has been observed as far as the authors are aware.

Another sign indicating that the PE matrix interferes with the covalently bonded PEO crystallization behavior (besides the lower crystallinity degrees developed) is the lower melting points for the PEO block in the PE-*b*-PEO diblocks compared to that in the PB-*b*-PEO diblock copolymers (see Table 4).

Annealed samples were also evaluated by DSC (results not shown). In general, the A, B, and C types of crystallization exotherms are still present, indicating that some percolated MD still exist even after the thermal treatment has been applied. However, a reduction in the contribution of the higher crystallization populations (A and B) to the total enthalpy of crystallization of the PEO blocks was observed, and this reduction was more pronounced for the PB-*b*-PEO diblock copolymers, which is in agreement with the higher long-range order observed by TEM for the annealed systems. An increase in the area of the lowest crystallization exotherm (exotherm C) is consistent with a lower degree of PEO microdomain percolation. Changes in crystallization temperature are a consequence of rearrange-

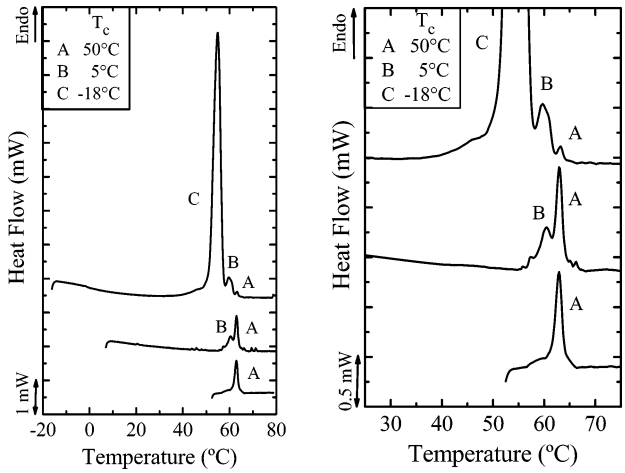

Figure 8. Final heating scans after $B_{81}EO_{19}^{34}$ was crystallized isothermally employing three different thermal treatments. On the right hand side figure, a close-up of the left hand side DSC scans is represented. See text for details.

ment of microdomains that modify the heterogeneities effectiveness and availability. The melting temperature of PEO blocks within PE-*b*-PEO remain lower than that in the PB-*b*-PEO, confirming the disturbing effect of PE on PEO crystallization as explained above. Fractionated melting was also seen although as expected the enthalpy of melting of the highest temperature melting population has correspondingly decreased compared to the case of unannealed samples.

In order to understand the origin of the fractionated melting observed for the PEO block within the copolymers, we performed sequential isothermal crystallization experiments. By crystallization of the samples at different temperatures, it is possible to separate different crystal populations, namely, those crystallizing in Figure 6 in exotherms A, B, and C. Each population is associated to a crystallization temperature that produces a specific melting temperature and in this particular case, since they are well spaced, they may not overlap with each other.

Figure 8 shows final heating scans after $B_{81}EO_{19}^{34}$ was crystallized isothermally employing three different thermal treatments: (a) One isothermal crystallization step. The sample was isothermally crystallized after quenching from the melt to 50 °C where the sample was held for 15 min. After this time was elapsed, the sample was heated from 50 to 80 °C in order to melt the crystals formed during the isothermal crystallization. In this case, 50 °C corresponds to a very low supercooling which was deliberately chosen to produce the crystallization of MD containing the most active type A heterogeneities (see Figure 6 *right*). Only one sharp melting peak labeled A was obtained as expected. (b) Two sequential crystallization steps. The sample was first crystallized at 50 °C for 15 min (the isothermal crystallization times were selected in order to obtain saturation levels of crystallinity at any given T_c) and then quenched to 5 °C where it was held for an additional 5 min for isothermal crystallization. This second successive crystallization step was designed to try to crystallize the sphere population that contains type B heterogeneities (see Figure 6 right). The sample was then heated from 5 to 80 °C and this heating scan is shown in Figure 8. A bimodal melting can be observed reflecting the fusion of the populations of the two spheres that crystallized at 5 °C (B) and 50 °C (A). (c) Three sequential crystallization steps. The sample was first crystallized at 50 °C for 15 min, then at 5 °C for 5 min, and then finally rapidly quenched to −18 °C where it was left to isothermally crystallize for 40 min.

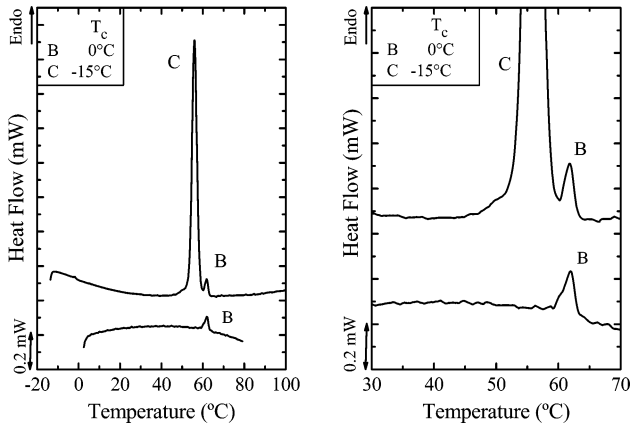

Figure 9. Final heating scans after $B_{89}EO_{11}^{105}$ was crystallized isothermally employing two different thermal treatments. On the right hand side figure, a close-up of the left hand side DSC scans is represented. See text for details.

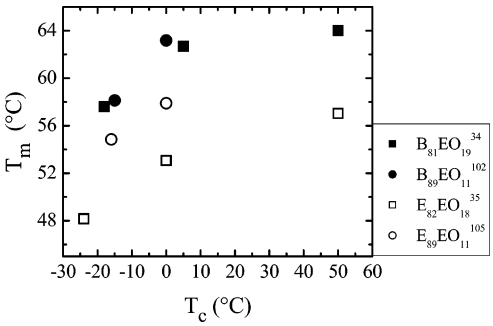

Figure 10. Melting temperatures for all PEO blocks obtained as a function of the isothermal crystallization temperature applied during the sequential crystallization process (as in Figures 8 and 9).

This third successive crystallization step was chosen to isothermally crystallize the majority of the isolated PEO MDs within $B_{81}EO_{19}^{34}$ which can only crystallize at very large supercoolings (see Figure 6 right). The DSC heating scan after such sequential isothermal crystallization can also be seen in Figure 8 (top trace). Fractionated melting with three different well spaced peaks can be observed corresponding to the three sequential isothermal crystallization steps. It is noteworthy that fraction B is now more abundant than fraction A, a fact that may be related to the reorganization or annealing during the heating scan. It is very clear, as it is in Figure 6, that the dominant melting endotherm corresponds to the fusion of superficially or homogeneously nucleated MD (population C).

The same effect of fractionated melting was obtained in $B_{89}EO_{11}^{102}$ (Figure 9) but only two melting fractions are present, in comparison to $B_{81}EO_{19}^{34}$. Since in this case we were not able to crystallize spheres at 50 °C, we attribute this effect to the absence of a high enough number of spheres containing type A heterogeneities. Once more the dominant melting process corresponds to the fusion of superficially or homogeneously isolated spheres. Similar behaviors were observed for both hydrogenated copolymers $E_{82}EO_{18}^{35}$ and $E_{89}EO_{11}^{105}$ (results not shown).

Figure 10 presents the peak melting points of all PEO block crystalline fractions obtained as a function of the isothermal crystallization temperature applied during the sequential crystallization process described above. As expected, the apparent melting points increase with T_c and increase with PEO molecular weight. A very interesting result is that the melting points for the PEO within PE-*b*-PEO are always lower compared to that of PEO within PB-*b*-PEO. This indicates that these PEO crystals

Table 5. Avrami Parameters of the PEO Block within Diblock Copolymers Obtained by ISC at Different Temperatures

	T_c (°C)	n	k (min^{-n})	$\tau_{50\%,exp}$ (min)	$\tau_{50\%,theo}$ (min)	R^2
$B_{81}EO_{19}$[34]	50	1.2864	2.1868	0.4	0.41	0.9925
$B_{81}EO_{19}$[34]	−18	1.2705	0.2910	2.2	1.98	0.9969
$B_{89}EO_{11}$[102]	0	1.8009	2.0977	0.7	0.54	0.9977
$B_{89}EO_{11}$[102]	−15	1.0177	0.0318	21.7	20.69	0.9998
$E_{82}EO_{18}$[35]	−24	1.2313	0.6746	1.2	1.02	0.9954
$E_{89}EO_{11}$[105]	−16	0.9560	0.1988	3.5	3.69	0.9880

are less stable from a thermodynamic point of view since they are most likely composed of thinner lamellae. Once more the results obtained in this work suggest that the PE semicrystalline matrix (despite its low degree of crystallinity, see Table 4) interferes with the crystallization of the PEO block imposing some topological restrictions. The results in Table 4 have already indicated that during the DSC cooling scans from the melt the PEO spheres formed by the PEO block within PE-*b*-PEO have a lower degree of crystallinity than those formed by the PEO block within PB-*b*-PEO. We can therefore conclude that the PE matrix exerts a higher degree of interference with PEO crystallization than the PB matrix.

Variations in the T_m of PEO blocks were also found by Bailey et al.[45] and Epps et al.[46] in polyisoprene-*b*-polystyrene-*b*-poly(ethylene oxide) (PI-*b*-PS-*b*-PEO) and PS-*b*-PI-*b*-PEO. With PS/PI ratio remaining constant, the T_m of the PEO block was lower when it was directly attached to PS instead of to PI. This behavior was attributed to the glassy character of the PS block, whereas PI is rubbery at the T_c of PEO. Additionally, reductions in T_m as domain spacing of PEO microphases decreases within the same systems have been reported for PB-*b*-PI-*b*-PEO,[7] PI-*b*-PS-*b*-PEO, and PS-*b*-PI-*b*-PEO[45,46] triblock terpolymers.

Isothermal Crystallization Kinetics. In order to get insight into the nucleation and crystallization kinetics of the crystallization process, the Avrami equation was used to fit the transformation process.[47−53] The evolution of enthalpy with time was followed by isothermal step crystallization (ISC), following closely the procedure reported in ref 51. Table 5 presents the results.

In general the Avrami indexes encountered are rather low, and they mostly decrease with the crystallization temperature. In particular, the value obtained for the crystallization at 50 °C in the case of $B_{81}EO_{19}$[34] of 1.28 seems low for either percolated MD or heterogeneously nucleated PEO. Not only the percolation but also the volume of percolated material influences the rate of transformation. However, an Avrami index of $n = 1.6$ was reported by Loo et al.[14] in a percolated system, and the result was attributed to a sigmoidal crystallization kinetics in a crystallization-destroyed sphere lattice microdomain of a PE block within poly(high-1,4-butadiene)-*b*-poly-(styrene-*ran*-butadiene) diblock copolymers.

For those cases where the PEO MDs are crystallizing at the lowest temperatures employed (where probably isolated spheres are being crystallized without heterogeneities), the Avrami indexes obtained are 1.27, 1.01, 1.23, and 0.96. These can be approximated to an Avrami index value of 1 or a first order overall crystallization kinetics. These have been found in the literature before in the case of isolated microdomains, and the interpretation given to this result is that the kinetics is entirely controlled by the nucleation process since the crystal growth from the nucleus to the interphase can be regarded as instantaneous (see ref 14). This result confirms the interpretation that the exotherm C in Figure 6b is due to the crystallization of heterogeneity-free isolated droplets that are either superficially or homogeneously nucleated.

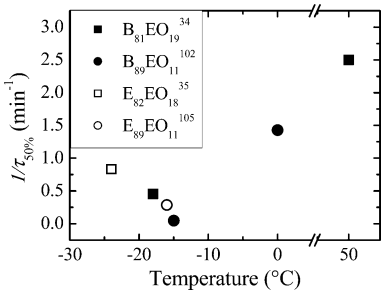

Figure 11. Inverse of the experimentally determined half-crystallization time as a function of isothermal crystallization temperature for PB-*b*-PEO and PE-*b*-PEO diblock copolymers.

The fractionated crystallization phenomenon brings about crystallization exotherms at very large supercoolings. In the case of PEO, its equilibrium melting point temperature[54] is 69 °C and the T_g values associated to the β relaxation exhibit a range of −50 to −60 °C.[2,15] The determination of crystallization kinetics in a temperature range from 50 to −24 °C allows the estimation of kinetic parameters under conditions where the energetic barriers associated with the creation of primary nuclei and the transport of chains for the formation of such nuclei may significantly vary. Figure 11 shows how the inverse of the experimentally determined half-crystallization time (i.e., a measure of the overall crystallization rate) as a function of the isothermal crystallization temperature. For both $B_{81}EO_{19}$[35] and $B_{89}EO_{11}$[102], a reduction in overall crystallization rate can be seen as T_c decreases.

Since the Avrami index is generally close to 1, as a first approximation, we will consider a primary nucleation model to interpret the data presented in Figure 11. If we consider that the kinetics is dominated only by nucleation, we should take into account the usual dependence of nucleation rate on temperature, as proposed by Turnbull and Fisher:[55]

$$I^* = (NkT/h)\exp[-(\Delta G^* + \Delta G_\eta)/kT] \qquad (6)$$

where I^* is the nucleation rate in nuclei/s, N the number of noncrystallized chain elements that can participate in a single nucleation step, ΔG^* is the free energy for the formation of a critical size nucleus, and ΔG_η is the free energy term for the short-range diffusion of crystallizable chain elements through the interphase. According to the above equation, the nucleation process depends on two contributing factors. The first one depends on ΔG^* whose magnitude decreases with the supercooling, while the second one depends on ΔG_η, a term practically constant at high temperatures, but which increases significantly as the temperature approaches T_g. Since T_c is definitely approaching the T_g of the PEO in Figure 11, the reduction in overall crystallization rate can be interpreted as a reduction in nucleation rate due to the increase in ΔG_η.

Another interesting aspect that can be observed in Figure 11 and Table 5 is that the overall crystallization rates at temperatures of −15 and −16 °C are faster for the PEO spheres in a PE matrix than for equivalent spheres in a PB matrix. This is a very peculiar effect, since we have shown above that the PE matrix imposes a higher degree of topological restrictions on PEO as compared to PB, resulting in lower crystallinities and lower melting points. However, it seems that the thinner crystals formed in smaller amounts by the PEO in the PE matrix are formed at relatively higher rates. This experimental fact needs further study to ascertain its origin.

If the isothermal crystallization data is interpreted also in terms of secondary nucleation,[56] a similar conclusion can be

reached as above, i.e., secondary crystallization process can experience a significant retardation as T_g is approached and thus can explain the behavior shown by the experimental data in Figure 11.

Conclusions

In this work, the influence of the morphology on the crystallization process of PB-*b*-PEO diblock copolymers and their hydrogenated counterparts PE-*b*-PEO were studied by TEM, SAXS, and DSC. For the $B_{89}EO_{11}$[105] diblock copolymer and its hydrogenated version, PEO spheres were dispersed in a disordered fashion within a PB or a PE matrix. In the case of $B_{81}EO_{19}$[34] and $E_{82}EO_{18}$[35], a morphology of spheres and coalesced spheres was observed by TEM, while SAXS results indicated a mixed morphology of spheres and cylinders in view of the transitional composition employed. The degree of segregation strength in both types of diblock copolymers is comparable according to estimations based on the calculation of χ from solubility parameters. However, the PB-*b*-PEO systems exhibited a higher degree of order in the melt according to SAXS results. The study of the crystallization process by DSC revealed a marked fractionated crystallization phenomenon of the PEO block for all the copolymers studied here. The observation of different exotherms that were well separated in temperature in the cooling scans also allowed the observation of multiple fusion endotherms for the PEO block during subsequent heating scans. These different endotherms (fractionated melting) are a consequence of the formation of lamellar crystals of different thicknesses and thermodynamic stability whose reorganization capacity during the scans are limited. The correspondence between the different crystallization and fusion processes was carefully demonstrated by performing cumulative isothermal crystallization treatments on the samples followed by immediate heating scans. Isothermal crystallization results evidenced a first-order crystallization kinetics that indicates the preponderance of nucleation over growth as the dominant step in the solidification process of the PEO isolated MD. At large supercoolings, the half-crystallization times increased with the decrease in crystallization temperature. This was explained by the increase in the energy barrier associated with the transport term or molecular diffusion to the nucleation sites when crystallization temperatures approach the glass transition temperature of PEO. The thermodynamic stability of the PEO block crystals is lower when the matrix is a PE block and their crystallization rate is higher than when the matrix is a PB block.

References and Notes

(1) Hamley, I. W. *The Physics of Block Copolymers*; Oxford University Press: Oxford, 1998.
(2) Müller, A. J.; Balsamo, V.; Arnal, M. L. *Adv. Polym. Sci.* **2005**, *190*, 1−63.
(3) Quiram, D. J.; Register, R. A.; Marchand, G. R. *Macromolecules* **1997**, *30*, 4551−4558.
(4) Hamley, I. W. *Adv. Polym. Sci.* **1999**, *148*, 114−137.
(5) Loo. Y.-L.; Register, R. A. In *Developments in Block Copolymer Science*; Hamley, I. W., Ed.; Wiley: Chichester, 2004.
(6) Quiram, D. J.; Register, R. A.; Marchand, G. R.; Ryan, A. J. *Macromolecules* **1997**, *30*, 8338−8343.
(7) Schmalz, H.; Knoll, A.; Müller, A. J.; Abetz, V. *Macromolecules* **2002**, *35*, 10004−10013.
(8) Hamley, I. W.; Fairclough, J. P. A.; Terrill, N. J.; Ryan, A. J.; Lipic, P. M.; Bates, F. S.; Towns-Andrews, E. *Macromolecules* **1996**, *29*, 8835−8843.
(9) Manaure, A. C.; Morales, R. A.; Sánchez, J. J.; Müller, A. J. *J. Appl. Polym. Sci.* **1997**, *66*, 2481−2493; Arnal, M. L.; Matos, M. E.; Morales, R. A.; Santana, O. O.; Müller, A. J. *Macromol. Chem. Phys.* **1998**, *199*, 2275−2288; Molinuevo, C. H.; Mendez, G. A.; Müller A. J. *J. Appl. Polym. Sci.* **1998**, *70*, 1725−1735; Arnal, M. L.; Müller, A. J. *Macromol. Chem. Phys.* **1999**, *200*, 2559−2576.
(10) Manaure, A.; Müller, A. J. *Macromol. Chem. Phys.* **2000**, *201*, 958−972; Arnal, M. L.; Müller, A. J.; Maiti, P.; Hikosaka, M. *Macromol. Chem. Phys.* **2000**, *201*, 2493−2504.
(11) Loo, Y. L.; Register, R. A.; Ryan, A. J. *Macromolecules* **2002**, *35*, 2365−2374.
(12) Gedde, U. W. *Polymer Physics*; Chapman and Hall: London, 1995.
(13) Lorenzo, A. T.; Arnal, M. L.; Müller, A. J.; Boschetti, de Fierro, A.; Abetz, V. *Europ. Polym. J.* **2006**, 42, 516−533; Lorenzo, A. T.; Arnal, M. L.; Müller, A. J.; Boschetti-de-Fierro, A.; Abetz, V. *Macromolecules* **2007**, *40*, 5023−5037.
(14) Loo, Y. L.; Register, R. A; Ryan, A. J; Dee G. T. *Macromolecules* **2001**, *34*, 8968−8977.
(15) Arnal, M. L.; Balsamo, V.; López-Carrasquero, F.; Contreras, J.; Carrillo, M.; Schmalz, H.; Abetz, V.; Laredo, E.; Müller, A. J. *Macromolecules* **2001**, *34*, 7973−7982.
(16) Müller, A. J.; Arnal, M. L.; López-Carrasquero, F. *Macromol. Symp.* **2002**, *183*, 199−204.
(17) Nojima, S.; Toei, M.; Hara, S.; Tanimoto, S.; Sasaki, S. *Polymer* **2002**, *43*, 4087−4090.
(18) Müller, A. J.; Balsamo, V.; Arnal, M. L.; Jakob, T.; Schmalz, H.; Abetz, V. *Macromolecules* **2002**, *35*, 3048−3058.
(19) Schmalz, H.; Müller, A. J.; Abetz, V. *Macromol. Chem. Phys.* **2003**, *204*, 111−124.
(20) Müller, A. J.; Balsamo, V.; Arnal, M. L. In *Progress in Understanding of Polymer Crystallization*; Reiter, G., Strobl, G., Eds.; *Lecture Notes in Physics*; Springer: Berlin, Germany, 2007; Vol. 714, pp 229−259.
(21) Nandan, B.; Hsu, J.-Y.; Chen, H.-L. *J. Macromol. Sci., Part C* **2006**, *46*, 143−172.
(22) Albuerne, J.; Márquez, L.; Müller, A. J.; Raquez, J. M.; Degée, Ph.; Dubois, Ph.; Castelletto, V.; Hamley, I. *Macromolecules*, **2003**, *36*, 1633−1644.
(23) Müller, A. J.; Albuerne, J.; Márquez, L.; Raquez, J.-M.; Degée, Ph.; Dubois, Ph.; Hobbs, J.; Hamley, I. W. *Faraday Discuss.* **2005**, *128*, 231−252; Hamley, I. W.; Castelletto, V.; Castillo, R. V.; Müller, A. J.; Martin, C. M.; Pollet, E.; Dubois, Ph. *Macromolecules* **2005**, *38*, 463−472; Hamley, I. W.; Parras, V. P.; Castelletto, V.; Castillo, R. V.; Müller, A. J.; Pollet, E.; Dubois, Ph.; Martin, C. M. *Macromol. Chem. Phys.* **2006**, *207*, 941−953.
(24) Chen, H.-L.; Hsiao, S.-C.; Lin, T.-L.; Yamauchi, K.; Hasegawa, H.; Hashimoto, T. *Macromolecules* **2001,** *34*, 671−674.
(25) Massa, M. V.; Carvalho, J. L.; Dalnoki-Veress, K. *Eur. Phys. J. E.* **2003**, *12*, 111−117.
(26) Chen, H.-L.; Li, H.-C.; Huang, Y.-Y.; Chiu, F.-Ch. *Macromolecules* **2002**, *35*, 2417−2422.
(27) Reiter, G.; Castelein, G.; Sommer, J.-U. *Phys. Rev. Lett.* **2001**, *87*, 226101-1−226101-4.
(28) Röttele, A.; Thurn-Albrecht, T.; Sommer, J.-U.; Reiter, G. *Macromolecules* **2003**, *36*, 1257−1260.
(29) Huang, Y.-Y.; Chen, H.-L.; Li, H.-C.; Lin, T.-L.; Lin, J.-S. *Macromolecules* **2003**, *36*, 282−285.
(30) Huang, Y.-Y.; Yang, C.-H.; Chen, H.-L.; Chiu, F.-C.; Lin, T.-L.; Liou, W. *Macromolecules* **2004**, *37*, 486−493.
(31) Sun, L.; Liu, Y.; Zhu, L.; Hsiao, B. S.; Avila-Orta, C. A. *Polymer* **2004**, *45*, 8181−8193.
(32) Sun, L.; Liu, Y.; Zhu, L.; Hsiao, B. S.; Avila-Orta, C. A. *Macromol. Rapid Commun.* **2004**, *25*, 853−857.
(33) Boschetti-de-Fierro, A.; Müller, A. J.; Abetz, V. *Macromolecules* **2007**, *40*, 1290−1298; Boschetti-de-Fierro, A.; Spindler, L.; Reiter, G.; Olmos, D.; Magonov, S.; Abetz, V. *Macromolecules* **2007**, *40*, 5487−5496.
(34) Schmalz, H.; Abetz, V.; Lange, R.; Soliman, M. *Macromolecules* **2001**, *34*, 795−800.
(35) Schmalz, H.; Böker, A.; Lange, R.; Krausch, G.; Abetz, V. *Macromolecules* **2001**, *34*, 8720−8729.
(36) Tang, C. C.; Martin, C. M.; Laundy, D.; Diakun, G. P. *Nucl. Instrum. Methods Phys. Res., Sect. B* **2004**, *222*, 659−666.
(37) Cernik, R. J.; Barnes, P.; Bushnell-Wye, G.; Dent, A. J.; Diakun, G. P.; Flaherty, J. V.; Greaves, G. N.; Heeley, E. L.; Helsby, W.; Jacques, S. D. M.; Kay, J.; Rayment, T.; Ryan, A. J.; Tang, C. C.; Terrill, N. J. *J. Synchrotron Radiat.* **2004**, *11*, 163−170.
(38) Balsamo, V.; Urdaneta, N.; Pérez, L.; Carrizales, P.; Abetz, V.; Müller, A. J. *Eur. Polym. J.* **2004**, *40*, 1033−1049.
(39) Chandrasekar, S. *Rev. Mod. Phys*., **1943**, *15*, 1−36.
(40) Feigin, L. A.; Svergun, D. I. *Structure Analysis by Small-Angle X-ray and Neutron Scattering*; Plenum Press: New York, 1987. Cited by ref 26.
(41) Van Krevelen, D. W. In *Properties of Polymer*, 3rd ed.; Elsevier: Amsterdam, 1997; Chapter 7, p 189.
(42) Almdal, K.; Hillmyer, M. A.; Bates, F. S. *Macromolecules* **2002**, *35*, 7685−7691.

(43) Mathot, V. B. F. *Calorimetry and Thermal Analysis of Polymers*; Hanser Publisher: New York, 1994.
(44) Müller, A. J.; Arnal, M. L. *Prog. Polym. Sci*. **2005**, *30*, 559−603.
(45) Bailey, T. S.; Pham, H. D.; Bates, F. S. *Macromolecules* **2001**, *34*, 6994−7008.
(46) Epps, T. H., III.; Bailey, T. S.; Waletzko, R.; Bates, F. S. *Macromolecules* **2003**, *36*, 2873−2881.
(47) Mandelkern, L.; Alamo, R. G. Thermodynamic quantities governing melting. In *Physical properties of polymers handbook*; Mark, J. E., Ed.; American Institute of Physics: Woodbury, 1996; p 119.
(48) Avrami, M. *J. Chem. Phys.* **1941**, *9*, 177−184.
(49) Evans, U. R. *Trans. Faraday Soc.* **1945**, *41*, 365−374.
(50) Piorkowska, E.; Galeski, A.; Haudin, J. M. *Prog. Polym. Sci.* **2006**, *31*, 549−575.
(51) Lorenzo, A. T.; Arnal, M. L.; Albuerne, J.; Müller, A. J. *Polym. Test.* **2007**, *26*, 222−231.
(52) Mandelkern, L. In *Physical Properties of Polymers*, 3rd ed.; Mark, J. E., Ed.; Cambridge University Press: Cambridge, 2004.
(53) Shultz, J. M. In *Polymer Crystallization*; Oxford University Press: London, 2001.
(54) Runt, J. Crystallinity Determination. In *Encyclopedia of Polymer Science & Engineering*, 2nd ed.; Mark, H., Bikales, N., Overberger, C., Menges, J. Eds.; John Wiley & Sons: New York, 1987; Vol. 4, pp 482−519.
(55) Turnbull, D. and Fisher, J. C. *J. Chem. Phys.* **1949**, *17*, 71. Cited in Wunderlich B. *Macromolecular Physics;* Academic Press: New York, 1976; Vol. 2.
(56) Mandelkern, L. In *Crystallization of Polymers*, 2nd ed.; Cambridge University Press: Cambridge, 2002; Vol. 1.

MA0718907